Geosciences Journal
DOI 10.1007/s12303-014-0009-7

Mesoscopic study of the formation of pseudomorphs with presence of chemical fluids

Li Chen — *Key Laboratory of Thermo-Fluid Science and Engineering of MOE, School of Energy and Power Engineering, Xi'an Jiaotong University, Xi'an, Shaanxi 710049, China*
Qinjun Kang* — *Computational Earth Science Group (EES-16), Los Alamos National Laboratory, Los Alamos, NM 87544, USA*
Hailin Deng — *CSIRO Land and Water, Private Bag No. 5, Wembley WA 6913, Australia*
J. William Carey — *Earth System Observations Group (EES-14), Los Alamos National Laboratory, Los Alamos, NM 87544, USA*
WenQuan Tao — *Key Laboratory of Thermo-Fluid Science and Engineering of MOE, School of Energy and Power Engineering, Xi'an Jiaotong University, Xi'an, Shaanxi 710049, China*

ABSTRACT: A numerical approach is developed to simulate the formation of pseudomorphs with presence of chemical fluids at the mesoscopic scale. This approach consists of the lattice Boltzmann method (LBM) for transport of chemical species in the pore space, a chemical reaction model including basic kinetics of the coupled dissolution and precipitation reactions, and a mesoscopic model for nucleation and crystal growth. Our study confirms the mechanism of the solution chemistry-driven interface-coupled dissolution-precipitation for the formation of pseudomorphs and identifies several sources for the generation of porosity in the pseudomorphs. We demonstrate that epitaxial precipitation is not necessary and random crystal growth may be more favorable for pseudomorphs. We show that the difference of precipitation barrier on the surface of the primary and secondary minerals should not be too large. Otherwise only the rim of the primary phase is roughly preserved.

Key words: pseudomorph, precipitation, dissolution, reactive transport, lattice Boltzmann method

1. INTRODUCTION

Reactive transport involving precipitation and/or dissolution has attracted scientists in different fields due to the diverse patterns formed in these processes, such as Liesegang bands or rings (Chen et al., 2012a) and CO_2 storage in deep saline aquifers (Kang et al., 2010). Among these, the formation of pseudomorphs is of particular interest, in which the secondary phase (or phase assemblage) occupies the space previously occupied by the primary phase through chemical reaction, while preserving the overall outward morphology or even the fine internal textural details of the primary phase (Merino and Dewers, 1998; Spry, 1969). The pseudomorph reaction widely exists in nature (Putnis, 2002), for example replacement of dolomite by calcite in metasomatic processes (Tucker, 2001). It can also be found in engineering processes such as uptake of toxic cations from wastewater using zeolites (Inglezakis et al., 2002). Due to the distinct feature of the preservation of the shape of the primary phase, pseudomorphic replacement provides a novel way to synthesize new materials based on pre-shaped precursors and has potential applications in fabricating pure mineral materials (such as functional materials (Reboul et al., 2012)) that are difficult to synthesize using conventional routes.

Pseudomorphic replacement reactions in the presence of chemical fluids generally present the following distinctive features (Putnis, 2002): first and foremost, the overall shape and volume of the primary phase is inherited by the secondary phase; second, the secondary phase generated is usually porous; and third, there is a sharp reaction front between the primary and secondary phases. Conventionally, pseudomorphism has been considered as a strong argument for solid-state diffusion mechanism, as morphology of the primary phase is unlikely to be inherited if dissolution occurs. Besides, it is found that in some pseudomorphic replacement the reaction kinetics is of zero order which is not the case where dissolution and precipitation occur (Hunger and Benning, 2007). However, the last two features of the pseudomorphism, namely porous structures and sharp reaction front, indicate that the solid-state diffusion mechanism is unlikely to be a tenable mechanism (Harlov et al., 2011; Putnis, 2002; Xia et al., 2009). In addition, more delicate experiments using isotope tracer confirm that chemical bonds of the primary phase are broken and the whole structures are recrystallized (O'Neil and Taylor, 1967; Putnis and Putnis, 2007; Putnis and Mezger, 2004), further casting doubt on the mechanism of solid-state diffusion mechanism.

The mechanism of interface-coupled dissolution-precipitation has received increasing attention (Harlov et al., 2011; Merino et al., 1993; O'Neil and Taylor, 1967; Putnis and Austrheim, 2010; Putnis and Mezger, 2004; Putnis et al., 2007; Reboul et al., 2012; Xia et al., 2009). The co-location of dissolution and precipitation in pseudomorphism requires the equivalence between dissolution and precipitation rates. While Merino (Merino and Dewers, 1998; Merino et al., 1993) suggested that a local non-hydrostatic stress generated by

*Corresponding author: qkang@lanl.gov

crystal growth provides such equivalence, A. Putnis (Putnis, 2002) suggested that the equivalence stem from the local solution chemistry. The porosity in the secondary phase is very important as it provides pathways for the reactant in the bulk fluid to transport into the fluid boundary layer and thus allows the precipitation to continue (Putnis and Mezger, 2004). However, why the pores are generated is not answered by Merino (Merino and Dewers, 1998). A. Putnis (Putnis, 2002) pointed out that the porosity results from a volume deficit caused by either solubility difference or volume difference between the primary and secondary phases.

We intend to address several important issues related to the formation of pseudomorphism in this paper: How does the solution chemistry-driven interface-coupled dissolution-precipitation form the pseudomorph? Are there other sources for the porosity generation besides solubility difference or volume difference? Which kind of crystal growth mechanisms is favorable for the formation of pseudomorphs? How do the reaction kinetics affect the formation of pseudomorphs? Can we simulate pseudomorph growth processes to gain insight into fundamental mechanisms of crystal growth behavior? We base our research on a novel numerical approach consisting of the lattice Boltzmann method (LBM) for transport of chemical species in pore space (Chen et al., 2012a, b), a chemical reaction model including basic kinetics of the coupled dissolution and precipitation reactions, and a mesoscopic model for nucleation and crystal growth (Kang et al., 2004). It is worth mentioning that the pseudomorphism studied in the present study is restricted to that generated by pseudomorphic replacement reactions with the presence of chemical fluids. In nature, some pseudomorphic replacement reactions take place between a mineral pair without any common chemical species. Furthermore, a large crystal can be replaced by another one that does not have internal porosity. These pseudomorphisms are not in the scope of the present work.

2. PHYSICOCHEMICAL MODEL AND NUMIRCAL METHOD

2.1. Chemical Model

In the present study, we use a simplified chemical model containing the minimum number of constituents that adequately captures the key characteristics of pseudomorphic replacement reactions. This consists of three aqueous species ($A_{(aq)}$, $B_{(aq)}$ and $C_{(aq)}$), two solid phases ($D_{(s)}$ and $P_{(s)}$) and two reactions (dissolution and precipitation)

$$A_{(aq)} + D_{(s)} \rightleftharpoons B_{(aq)} \tag{1}$$

$$C_{(aq)} + B_{(aq)} \rightleftharpoons P_{(s)} \tag{2}$$

Equation (1) is the dissolution reaction in which aqueous $A_{(aq)}$ reacts with solid phase $D_{(s)}$ generating aqueous $B_{(aq)}$, and Equation (2) is the precipitation reaction in which $B_{(aq)}$ generated by Equation (1) reacts with another aqueous $C_{(aq)}$ leading to the secondary precipitate $P_{(s)}$. Since $B_{(aq)}$ is one of the elements of $P_{(s)}$ and is released by the dissolution reaction, the two reactions are closely coupled at the $D_{(s)}$-fluid interface. An example reaction would be the conversion of calcite to fluorite:

$$H^{+}_{(aq)} + CaCO_{3(s)} = Ca^{2+}_{(aq)} + HCO^{-}_{3(aq)} \tag{3a}$$

$$2F^{-}_{(aq)} + Ca^{2+}_{(aq)} = CaF_{2(s)} \tag{3b}$$

where the bicarbonate ion is lost from the system. This simplified chemical model is handy and efficient to study the transport and reaction kinetic parameters and to identify dominant processes and mechanisms for the formation of pseudomorphs.

2.2. Governing Equations

The governing equations for mass transport are

$$\frac{\partial C_{A_{(aq)}}}{\partial t} = D_{A_{(aq)}} \Delta C_{A_{(aq)}} \tag{4a}$$

$$\frac{\partial C_{B_{(aq)}}}{\partial t} = D_{B_{(aq)}} \Delta C_{B_{(aq)}} \tag{4b}$$

$$\frac{\partial C_{C_{(aq)}}}{\partial t} = D_{C_{(aq)}} \Delta C_{C_{(aq)}} \tag{4c}$$

where t is time, C is the concentration, and D is the diffusivity. Δ is the Laplace operator.

2.3. Precipitation

In the present study, the precipitation is regarded as a kinetically hindered, autocatalytic process, meaning that the precipitation reaction between $C_{(aq)}$ and $B_{(aq)}$ has two barriers. One is a kinetic barrier related to the kinetics of the nucleation process, and the other is a thermodynamic barrier with regard to crystal growth (Mullin, 2001). In this study, we do not consider homogeneous nucleation from the solution (which requires significant degrees of supersaturation to overcome the high surface energy (Mullin, 2001). We assume that the surface of the $D_{(s)}$ can act as a template that catalyzes the precipitation of $P_{(s)}$ after a model-defined degree of supersaturation is reached and thus crystal growth takes place on this surface or on the surface of $P_{(s)}$ once this thermodynamic barrier is overcome. Two thermodynamic barriers to crystal growth are introduced by $K_{c,D}$ on the existing surface of $D_{(s)}$ and $K_{c,P}$ on the surface of $P_{(s)}$. The values of these barriers are listed in Table 1.

The crystal growth process around an existing surface is simulated using the crystal growth model developed in Ref.

Table 1. Values of variables used in the simulations

Variable		Physical unit	Lattice unit
Diffusivity of A, B and C	D	1.0×10^{-9} m^2 s^{-1}	0.2
Molar volume of D	$\overline{V}_{m,\mathrm{D}}$	3.0×10^{-5} m^3 mol^{-1}	0.6
Molar volume of P	$\overline{V}_{m,\mathrm{P}}$	3.0×10^{-5} m^3 mol^{-1}	0.6
Inlet concentration of A	$C_{\mathrm{A,in}}$	2 M (2000 mol m^{-3})	0.1
Inlet concentration of B	$C_{\mathrm{B,in}}$	0 M	0
Inlet concentration of C	$C_{\mathrm{C,in}}$	2 M	0.1
Initial volume	V_0	5.0×10^{-5} m^3	1
Reaction constant of Reaction 1	k_1	1×10^{-1} mol m^{-2} s^{-1}	1×10^{-3}
Reaction constant of Reaction 2	k_2	1×10^{-3} mol m^{-2} s^{-1}	1×10^{-5}
Equilibrium constant of Reaction 1	K_1	1×10^{-2}	1×10^{-2}
Equilibrium constant of Reaction 2	K_2	1.25×10^{-3} m^6 mol^{-2}	5000
Thermokinetic barrier on D surface	$\mathrm{K_{c,D}}$	0.8×10^{5} mol^2 m^{-6}	2×10^{-4}
Thermokinetic barrier on P surface	$\mathrm{K_{c,P}}$	0.8×10^{5} mol^2 m^{-6}	2×10^{-4}

(Kang et al., 2002, 2003, 2004, 2006). On the surface of a precipitating node or an existing $\mathrm{D_{(s)}}$ node, $\mathrm{C_{(aq)}}$ and $\mathrm{B_{(aq)}}$ react, leading to the consumption of $\mathrm{C_{(aq)}}$ and $\mathrm{B_{(aq)}}$ in the vicinity and a change of the node density due to gain of $\mathrm{P_{(s)}}$. For generality, a simple kinetic reaction model is applied.

$$D_{\mathrm{C_{(aq)}}}\frac{\partial C_{\mathrm{C_{(aq)}}}}{\partial \mathbf{n}}=\begin{cases}0 \text{ if } C_{\mathrm{C_{(aq)}}}C_{\mathrm{B_{(aq)}}}<\mathrm{K_c}\\ -k_2(1-K_2C_{\mathrm{C_{(aq)}}}C_{\mathrm{B_{(aq)}}}) \text{ if } C_{\mathrm{C_{(aq)}}}C_{\mathrm{B_{(aq)}}}\geq\mathrm{K_c}\end{cases} \tag{5a}$$

$$D_{\mathrm{B_{(aq)}}}\frac{\partial C_{\mathrm{B_{(aq)}}}}{\partial \mathbf{n}}=\begin{cases}0 \text{ if } C_{\mathrm{C_{(aq)}}}C_{\mathrm{B_{(aq)}}}<\mathrm{K_c}\\ -k_2(1-K_2C_{\mathrm{C_{(aq)}}}C_{\mathrm{B_{(aq)}}}) \text{ if } C_{\mathrm{C_{(aq)}}}C_{\mathrm{B_{(aq)}}}\geq\mathrm{K_c}\end{cases} \tag{5b}$$

where k_2 and K_2 are the reaction rate and equilibrium constants, respectively. K_c is $K_{c,D}$ or $K_{c,P}$, depending on which surface the crystal growth takes place. High equilibrium constant means low solubility of $\mathrm{P_{(s)}}$. $\mathbf{n}$ is the direction normal to the surface pointing to the void space. Correspondingly, the volume of the node is updated by

$$\frac{\partial V_P}{\partial t}=-A\overline{V}_{\mathrm{m,P}}k_2(1-K_2C_{\mathrm{C_{(aq)}}}C_{\mathrm{B_{(aq)}}}) \tag{6}$$

where A is the reaction area, $\overline{V}_{\mathrm{m}}$ is the molar volume. The volume of $\mathrm{P_{(s)}}$ grows at the expense of $\mathrm{C_{(aq)}}$ and $\mathrm{B_{(aq)}}$, and the surface reaction continues as long as C_CC_B exceeds the crystal growth threshold (K_c). When the volume of this precipitate node exceeds a certain threshold value (in the present study $2V_0$, with V_0 as the initial volume), the crystal grows and one of the nearest neighboring fluid nodes of this node becomes a solid node. Then the volume of the precipitate node is set back to V_0; meanwhile the new formed node is assigned with an initial volume V_0 and is marked as a "crystal growth node (CGN)". Three rules are used to determine which one of the nearest neighboring fluid nodes will turn into a CGN. In the first rule the node is randomly chosen (random precipitation) (Kang et al., 2004). In the second rule the node with highest C_CC_B is chosen (concentration-controlled precipitation), thus the crystal growth is always towards the direction with highest C_CC_B (Chen et al., 2013b). In the third rule the node adjacent to the $\mathrm{D_{(s)}}$-fluid interface is chosen, thus the crystal tends to cover the surface of $\mathrm{D_{(s)}}$. The third rule is used to approximately mimic the epitaxial precipitation process in which the secondary phase tends to form a thin layer covering the surface of the primary phase.

2.4. Dissolution

On the surface of $\mathrm{D_{(s)}}$, a dissolution reaction takes place that consumes $\mathrm{A_{(aq)}}$ and releases $\mathrm{B_{(aq)}}$. This reaction is considered in the simulation through the surface reaction. Based on the canonical form of Equation (1): $\mathrm{B_{(aq)}}-\mathrm{A_{(aq)}}\rightleftarrows\mathrm{D_{(s)}}$, the following kinetic model can be used to describe the dissolution (Kang 2006).

$$D_{\mathrm{A_{(aq)}}}\frac{\partial C_{\mathrm{A_{(aq)}}}}{\partial n}=k_1\left(1-K_1\frac{C_{\mathrm{B_{(aq)}}}}{C_{\mathrm{A_{(aq)}}}}\right) \tag{7a}$$

$$D_{\mathrm{B_{(aq)}}}\frac{\partial C_{\mathrm{B_{(aq)}}}}{\partial n}=k_1\left(1-K_1\frac{C_{\mathrm{B_{(aq)}}}}{C_{\mathrm{A_{(aq)}}}}\right) \tag{7b}$$

where k_1 and K_1 are reaction rate and equilibrium constants, respectively. The volume of the corresponding surface $\mathrm{D_{(s)}}$ node is decreased as follows

$$\frac{\partial V_{\mathrm{D_{(s)}}}}{\partial t}=-A\overline{V}_{\mathrm{m,D}}k_1\left(1-K_1\frac{C_{\mathrm{B_{(aq)}}}}{C_{\mathrm{A_{(aq)}}}}\right) \tag{8}$$

If V_D reaches zero, this solid node is removed from the system and is converted to a fluid node.

2.5. Lattice Boltzmann Method

The governing equations of $A_{(aq)}$, $B_{(aq)}$ and $C_{(aq)}$ are solved using the LBM for solute transport (Chen et al., 2012a, b).

$$g_{\alpha k}(\mathbf{x}+\mathbf{e}_\alpha \delta t, t+\delta t) = g_{\alpha k}(\mathbf{x}, t) - \frac{1}{\tau_k}(g_{\alpha k}(\mathbf{x}, t) - g^{eq}_{\alpha k}(C_k, \mathbf{u})) \tag{9}$$

where $g_{\alpha k}$ is the distribution function of the *kth* component with velocity $\mathbf{e}_\alpha$ at the lattice site $\mathbf{x}$ and time t, and τ is the collision time related to the diffusivity. Here, we use the D2Q5 lattice model for solute transport, as it has been shown to have not only comparable accuracy with the D2Q9 model but also better computational efficiency (Chen et al., 2013a, 2013b, 2013c; Kang et al., 2006, 2007). The equilibrium distribution function g^{eq} takes the following form

$$g^{eq}_{\alpha k} = C_k J_{\alpha k} \tag{10}$$

J is given by

$$J_\alpha = \begin{cases} J_0, & \alpha = 0 \\ (1-J_0)/4, & \alpha = 1,2,3,4 \end{cases} \tag{11}$$

where the rest fraction J_0 can be selected from 0 to 1 to obtain different diffusivity. The equilibrium distribution function given by Equation (10) can cover a wide range of diffusivity by adjusting J_0, which is a prominent advantage of such an equilibrium distribution (Chen et al., 2013a, 2013b).

Species concentration C and diffusivity are obtained by

$$C_k = \sum g_{\alpha k} \tag{12}$$

$$D_k = \frac{1}{2}(1-J_0)(\tau_k - 0.5)\frac{\delta x^2}{\delta t} \tag{13}$$

where δx is the length of one lattice.

2.6. Computational Domain and Numerical Method

Our model is defined on a two-dimensional 200×90 μm channel at the center of which is located a 100×30 μm $D_{(s)}$ grain. Initially the domain is filled with $A_{(aq)}$ and $B_{(aq)}$ in equilibrium with $D_{(s)}$ and is free of $C_{(aq)}$. Then, a solution including only $A_{(aq)}$ and $C_{(aq)}$ is introduced at the left entrance. Subsequently, $D_{(s)}$ dissolves and releases $B_{(aq)}$, leading to the supersaturated condition with respect of $P_{(s)}$ which then precipitates. The LBM introduced in Section 2.5 is used for reactive solute transport. The volume evolution Equations (6) and (8) are updated explicitly at each time step (Kang et al., 2006). The computational domain is discretized by 200×90 lattices with a resolution of 1 μm. The values of parameters used in the simulations are listed in Table 1. The crystal growth mechanism is random crystal growth mechanism, unless otherwise stated.

3. RESULTS AND DISCUSSION

3.1. Effect of Molar Volume Ratio

First the effect of molar volume ratio between $P_{(s)}$ and $D_{(s)}$ (denoted by φ) on the coupled dissolution and precipitation processes is investigated. The molar volume ratio (φ) is varied by changing the molar volume of $P_{(s)}$ while keeping that of $D_{(s)}$ fixed. The top three images in Figure 1 show the final geometries (Black denotes $D_{(s)}$ and Red $P_{(s)}$) at three values of molar volume ratio. As can be seen in Figure 1, a small molar volume of $P_{(s)}$ ($\varphi = 0.2$) leads to a severe volume deficit, generating sporadic precipitates with much porosity. Here, volume deficit means the total volume of precipitation is much lower than that of dissolution. Increasing φ to 0.5 results in precipitates $P_{(s)}$ with porous structures inheriting the overall shape of the primary phase $D_{(s)}$, and thus pseudomorphism takes place. The interconnected pores in such porous $P_{(s)}$ play an important role of allowing reactants in the bulk fluid to transport to the reaction front near the $D_{(s)}$-fluid interface. When φ is further increased to 1, these interconnected pores are lost, and the compact microstructures of $P_{(s)}$ completely separate $D_{(s)}$ from the bulk fluid. As a result, the dissolution is hindered by armoring of $P_{(s)}$, which in turn suppresses the precipitation due to coupled characteristics between these two reactions. The bottom image in Figure 1 shows the time evolution of the volume changes of $D_{(s)}$ and $P_{(s)}$ (normalized by the initial volume of $D_{(s)}$). The volume change denotes the difference between the initial volume and the volume at a certain time. The most important observation is that the dissolution is accelerated by the precipitation, by comparing the rate (slope of the curve) of the volume change of $D_{(s)}$ for coupled dissolution and precipitation reactions with that for the case containing only dissolution (precipitation is turned off). This is because the precipitation reaction consumes $B_{(aq)}$, and thus drives the dissolution reaction Equation (1) towards the right side. Therefore, the dissolution reaction is accelerated and releases more $B_{(aq)}$ which in turn facilitates the precipitation, leading to positive feedback between the precipitation and dissolution reactions.

Another important observation in Figure 1 is that the case of pseudomorphism ($\varphi = 0.5$) exhibits the highest dissolution rate as well as the largest amount of precipitate. This can be explained by the opposite effects of the precipitates on the coupled dissolution-precipitation processes, namely the positive effect of accelerating the dissolution reaction and the negative effect of hindering the transport of reactant. The porous structures of precipitates in the case of pseudomorphism are neither too compact nor too loose, leading to concordant dissolution and precipitation with the highest dissolution rate and the largest amount of precipitates. Such characteristics imply significant potential applications in the energy and environmental fields such as carbon dioxide mineral trap-

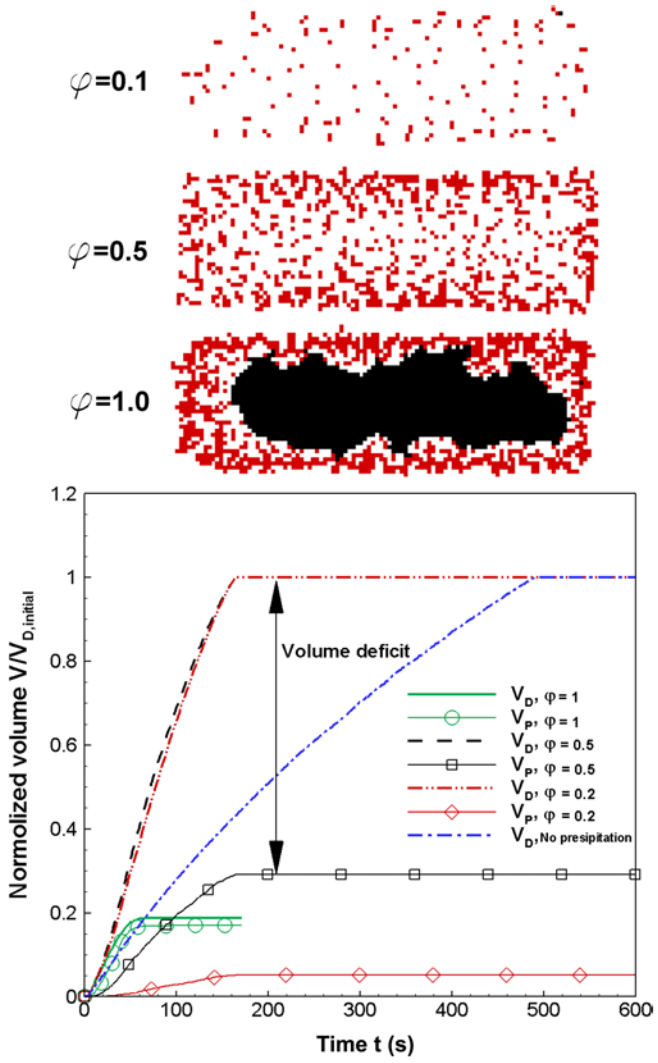

Fig. 1. Effects of molar volume ratio. Top three images: the final geometries of the primary phase ($D_{(s)}$) and the secondary phase ($P_{(s)}$) under different molar volume ratio of secondary phase to primary phase, φ. The dissolving primary phase is black and the precipitating secondary phase is red. Values of other parameters used are listed in Table 1. Bottom: time evolution of volume changes of the primary phase ($D_{(s)}$) and the secondary phase ($P_{(s)}$) under different molar volume ratios between the secondary phase and the primary phase. Values of other parameters used are listed in Table 1. Volume deficit means the difference between the volume variation of D and that of P.

ping (Daval et al., 2009) and uptake of toxic cations from polluted water (Inglezakis et al., 2002). Overall, the results here demonstrate the solution chemistry-driven interface-coupled dissolution-precipitation mechanism proposed by Putnis (Putnis, 2002) based on his experiments, and confirm the importance of the porosity in the secondary phase (Putnis and Putnis, 2007). In addition, the first origin of the volume deficit (or the porosity generated), namely the molar volume difference between the primary and secondary phases, is identified.

3.2. Effect of Equilibrium Constant, Reaction Rate Constant, and Concentration of Reactants

In addition to the molar volume, the final amount of the secondary phase generated also depends on the equilibrium constant of the secondary phase K_2, the reaction rate constant of precipitation k_2, and the concentration of reactants. We carried out a series of simulations under different conditions, and found that as K_2 (or k_2, or C_{in}) is increased, the morphologies of the precipitates change from sparse distributions, to pseudomorphic replacement, and to armoring, similar to the features observed as φ is increased. While the importance of molar volume and solubility differences between the primary and secondary phases have been emphasized in the literature as the origins of the volume deficit (Putnis and Putnis, 2007), the role of reaction rate and the concentrations of reactants have received less attention.

Since K_2, k_2, and C_{in} have similar effect as φ, the common belief that pseudomorphs are not possible when the molar volume of the second phase is greater than that of the primary phase is then questionable, because the effect of a high φ can be offset by a low value of other parameters. Indeed, in this study pseudomorphs are obtained by different combinations of the relevant parameters under such elevated molar volume ratio conditions, and Figure 2 shows one such case in which $\varphi = 1.2$, $C_{in,C} = 0.04$, $k_2 = 5\times10^{-6}$ and $K_2 = 4000$. In fact, it was also pointed out in (Putnis et al., 2007) that such a requirement on molar volume ratio is not necessary for pseudomorphic replacement .

3.3. Effect of Crystal Growth Mechanism

We next investigate the effects of crystal growth mechanisms, comparing random growth with concentration-controlled precipitation and epitaxial precipitation in Figure 3. These results were obtained with all other parameters set the same as the random growth result shown in Figure 1. The different precipitation mechanisms generate completely different morphologies of the precipitates. For concentration-controlled precipitation (Fig. 3a), the precipitates form structures oriented towards the surface of $D_{(s)}$. This is

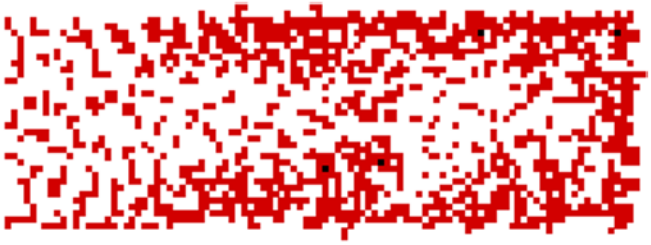

Fig. 2. Pseudomorph formed for the case in which the molar volume of the secondary phase is larger than the primary phase. $\varphi = 1.2$, $C_{in,C} = 0.04$, $k_2 = 5\times10^{-6}$ and $K_2 = 4000$. The dissolving primary phase is black and the precipitating secondary phase is red.

Fig. 3. The final geometries of the primary phase ($D_{(s)}$) and the secondary phase ($P_{(s)}$) under different crystal growth mechanisms: (a) concentration-controlled precipitation and (b) epitaxial precipitation. The dissolving primary phase is black and the precipitating secondary phase is red. The values of all the parameters are the same as those in Figure 1.

expected because $C_B C_C$ is higher near the $D_{(s)}$-fluid interface as $B_{(aq)}$ is released there. For epitaxial precipitation, the precipitates tend to grow on and cover the surface of $D_{(s)}$, thus completely ceasing the coupled reactions (Fig. 3b).

Note that epitaxial precipitation is usually considered to be crucial for the crystallographically oriented replacement of the primary phase by the secondary phase (Putnis, 2002; Xia et al., 2009). Here, based on our simulation results, we argue that epitaxial precipitation is not always needed for pseudomorphic replacement. First, epitaxial precipitation requires similar crystallographic structures between the primary and secondary phases, but pseudomorphism also takes place in systems where the precipitates have quite different structures from the primary phase (Putnis and Putnis, 2007). Second, we have found that in epitaxial precipitation processes the secondary phase tends to precipitate on the surface of the primary phase, which can efficiently and quickly passivate the underlying surface of the primary phase, thus arresting both dissolution and precipitation (Cubillas et al., 2005). In contrast, random heterogeneous nucleation and growth help form porous structures in the precipitates (Cubillas et al., 2005), allowing the underlying dissolution to continue which in turn sustains the precipitation. Third, the interface-coupled dissolution and precipitation processes have already guaranteed that the precipitates always locate near the dissolution sites (where the highest supersaturated conditions exist with respect to the secondary phase), thus generating precipitates that preserve the morphology of the primary phase. In conclusion, although epitaxial precipitation indeed takes place in situations where the primary and secondary phases have similar structures, it is not required for the formation of pseudomorphs.

3.4. Effect of Thermodynamic Barrier

The thermodynamic barrier to crystal growth on different solid surfaces may vary due to different surface energy. In the following calculations, we increase the degree of supersaturation conditions required for precipitation on the surface of the primary phase (while fixing that of the secondary phase), meaning that precipitation is favored on existing secondary phases. Figures 4a and b show the final geometries of $P_{(s)}$ and $D_{(s)}$ with thermodynamic barrier on $D_{(s)}$ surface as $3K_{c,D}$ and $2K_{c,D}$ ($K_{c,D}$ is listed in Table 1), respectively, with values of other parameters the same as those in Figure 1. In this figure we distinguish between precipitates forming on the dissolving primary phase (red) and those forming on a precipitating secondary phase (blue). Two important observations can be obtained by comparing images in Figure 4 with Figure 1. First, as precipitation on the surface of primary phase becomes more difficult, less precipitation occurs directly on the surface of the primary phase and precipitates growing on the existing secondary phase are increasingly common, resulting in coarser crystals with larger aggregates. Second, as precipitation on the surface of the primary phase becomes more difficult, only the rim of the primary phase is roughly preserved while the inner part is lost and becomes void. These simulations clearly explain similar observations obtained in recent experiments (Xia et al., 2009) where precipitation on the primary phase becomes rate-limited. The results here suggest that generation of pseudomorphs requires that the difference of precipitation barrier on the surface of the primary and secondary phases should not be too large.

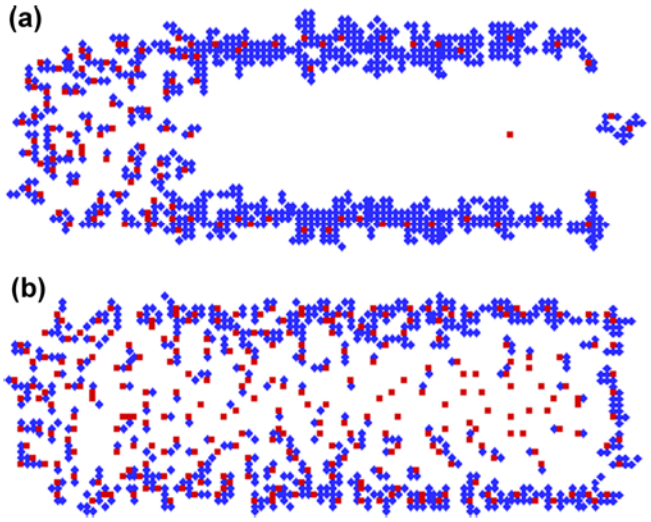

Fig. 4. The final geometries of the primary phase ($D_{(s)}$) and the secondary phase ($P_{(s)}$) with different thermodynamic barriers to growth on the surface of the primary phase: (a) $3K_{c,D}$ and (b) $2K_{c,D}$. The precipitates forming on the dissolving primary phase are red and those forming on a precipitating secondary phase are blue. In both cases, all of the primary phase is consumed. The values of all the parameters are the same as those in Figure 1.

4. CONCLUSION

A mesoscopic model is proposed for predicting reactive transport processes involving dissolution and precipitation. The model is able to reproduce diverse precipitation morphologies observed in experiments and in nature. With emphasis on the formation of pseudomorphs, we demonstrated for the first time by numerical simulation that a solution chemistry-driven interface-coupled dissolution-precipitation mechanism combined with volume deficit, proper precipitation mechanism, and low precipitation barrier on the surface of the primary phase is able to produce pseudomorphs.

ACKNOWLEDGMENTS: This work was supported by the key project of NNSFC (51136004), and the LDRD Program of Los Alamos National Laboratory.

REFERENCES

Chen, L., Kang, Q., He, Y., and Tao, W., 2012a, Mesoscopic study of the effect of gel concentration and material on the formation of precipitation patterns. Langmuir, 28, 11745–11754.

Chen, L., Kang, Q., He, Y., and Tao, W., 2012b, Pore-scale simulation of coupled multiple physicochemical thermal processes in micro reactor using lattice Boltzmann method. International Journal of Hydrogen Energy, 37, 13943–13957.

Chen, L., He, Y.-L., Kang, Q., and Tao, W.-Q., 2013a, Coupled numerical approach combining finite volume and lattice Boltzmann methods for multi-scale multi-physicochemical processes. Journal of Computational Physics, 255, 83–105.

Chen, L., Kang, Q., Robinson, B.A., He, Y.-L., and Tao, W.-Q., 2013b, Pore-scale modeling of multiphase reactive transport with phase transitions and dissolution-precipitation processes in closed systems. Physical Review E, 87, 043306.

Chen, L., Feng, Y.-L., Song, C.-X., Chen, L., He, Y.-L., and Tao, W.-Q., 2013c, Multi-scale modeling of proton exchange membrane fuel cell by coupling finite volume method and lattice Boltzmann method. International Journal of Heat and Mass Transfer, 63, 268–283.

Cubillas, P., Köhler, S., Prieto, M., Causserand, C., and Oelkers, E.H., 2005, How do mineral coatings affect dissolution rates? An experimental study of coupled $CaCO_3$ dissolution—$CdCO_3$ precipitation. Geochimica et Cosmochimica Acta, 69, 5459–5476.

Daval, D., Martinez, I., Corvisier, J., Findling, N., Goffé, B., and Guyot, F., 2009, Carbonation of Ca-bearing silicates, the case of wollastonite: Experimental investigations and kinetic modeling. Chemical Geology, 265, 63–78.

Harlov, D.E., Wirth, R., and Hetherington, C.J., 2011, Fluid-mediated partial alteration in monazite: the role of coupled dissolution–reprecipitation in element redistribution and mass transfer. Contributions to Mineralogy and Petrology, 162, 329–348.

Hunger, S. and Benning, L.G., 2007, Greigite: a true intermediate on the polysulfide pathway to pyrite. Geochemical Transactions, 8, 1–20.

Inglezakis, V.J., Loizidou, M.D., and Grigoropoulou, H.P., 2002, Equilibrium and kinetic ion exchange studies of Pb^{2+}, Cr^{3+}, Fe^{3+} and Cu^{2+} on natural clinoptilolite. Water Research, 36, 2784–2792.

Kang, Q., Zhang, D., and Chen, S., 2003, Simulation of dissolution and precipitation in porous media. Journal of Geophyiscal Research, 108, B10, 2505.

Kang, Q., Lichtner, P.C., and Zhang, D., 2006, Lattice Boltzmann pore-scale model for multicomponent reactive transport in porous media. Journal of Geophysical Research, 111, B05203.

Kang, Q., Lichtner, P.C., and Zhang, D., 2007, An improved lattice Boltzmann model for multicomponent reactive transport in porous media at the pore scale. Water Resources Research, 43, W12S14.

Kang, Q., Zhang, D., Chen, S., and He, X., 2002, Lattice Boltzmann simulation of chemical dissolution in porous media. Physical Review E, 65, 036318.

Kang, Q., Zhang, D., Lichtner, P.C., and Tsimpanogiannis, I.N., 2004, Lattice Boltzmann model for crystal growth from supersaturated solution. Geophysical Research Letters, 31, L21604.

Kang, Q., Lichtner, P., Viswanathan, H., and Abdel-Fattah, A., 2010, Pore Scale Modeling of Reactive Transport Involved in Geologic CO_2 Sequestration. Transport in Porous Media, 82, 197–213.

Merino, E. and Dewers, T., 1998, Implications of replacement for reaction–transport modeling. Journal of Hydrology, 209, 137–146.

Merino, E., Nahon, D., and Wang, Y., 1993, Kinetics and mass transfer of pseudomorphic replacement: application to replacement of parent minerals and kaolinite by Al, Fe, and Mn oxides during weathering. American Journal of Science 293, 135–155.

Mullin, J.W., 2001, Crystallization. Butterworth-Heinemann, Oxford, 181 p.

O'Neil, J.R. and Taylor, H.P., 1967, The oxygen isotope and cation exchange chemistry of feldspars. American Mineralogist, 52, 1414–1437.

Putnis, A., 2002, Mineral replacement reactions: from macroscopic observations to microscopic mechanisms. Mineralogical Magazine, 66, 689–708.

Putnis, A. and Putnis, C.V., 2007, The mechanism of reequilibration of solids in the presence of a fluid phase. Journal of Solid State Chemistry, 180, 1783–1786.

Putnis, A. and Austrheim, H., 2010, Fluid-induced processes: metasomatism and metamorphism. Geofluids, 10, 254–269.

Putnis, C.V. and Mezger, K., 2004, A mechanism of mineral replacement: isotope tracing in the model system KCl-KBr-H_2O. Geochimica et Cosmochimica Acta, 68, 2839–2848.

Putnis, C.V., Geisler, T., Schmid-Beurmann, P., Stephan, T., and Giampaolo, C., 2007, An experimental study of the replacement of leucite by analcime. American Mineralogist, 92, 19–26.

Reboul, J., Furukawa, S., Horike, N., Tsotsalas, M., Hirai, K., Uehara, H., Kondo, M., Louvain, N., Sakata, O., and Kitagawa, S., 2012, Mesoscopic architectures of porous coordination polymers fabricated by pseudomorphic replication. Nature materials, 11, 717–723.

Spry, A., 1969, Metamorphic Textures. Pergamon Press, Oxford, 350 p.

Tucker, M.E., 2001, Sedimentary Petrology: an introduction to the origin of sedimentary rocks. Wiley-Blackwell, Oxford, 110 p.

Xia, F., Brugger, J., Chen, G., Ngothai, Y., O'Neil, B., Putnis, A., and Pring, A., 2009, Mechanism and kinetics of pseudomorphic mineral replacement reactions: A case study of the replacement of pentlandite by violarite. Geochimica et Cosmochimica Acta, 73, 1945–1969.

Manuscript received November 13, 2013
Manuscript accepted February 19, 2014